Asymmetric Stability among the Transmembrane Helices of Lactose Permease†

Michael Bennett,‡,§ Robert D'Rozario,§,|| Mark S. P. Sansom,*,|| and Philip L. Yeagle*,‡

Department of Molecular and Cell Biology, University of Connecticut, Storrs, Connecticut 06269, and Department of Biochemistry, University of Oxford, Oxford OX1 3QU, U.K.

Received February 20, 2006; Revised Manuscript Received April 28, 2006

ABSTRACT: Combining structure determinations from nuclear magnetic resonance (NMR) data and molecular dynamics simulations (MD) under the same environmental conditions revealed a startling asymmetry in the intrinsic conformational stability of secondary structure in the transmembrane domain of lactose permease (LacY). Eleven fragments, corresponding to transmembrane segments (TMs) of LacY, were synthesized, and their secondary structure in solution was determined by NMR. Eight of the TMs contained significant regions of helical structure. MD simulations, both in DMSO and in a DMPC bilayer, showed sites of local stability of helical structure in these TMs, punctuated by regions of conformational instability, in substantial agreement with the NMR data. Mapping the stable regions onto the crystal structure of LacY reveals a marked asymmetry, contrasting with the pseudosymmetry in the static structure: the secondary structure in the C-terminal half is more stable than in the N-terminal half. The relative stability of secondary structure is likely exploited in the transport mechanism of LacY. Residues supporting proton conduction are in more stable regions of secondary structure, while residues key to substrate binding are found in considerably unstable regions of secondary structure.

Lactose permease (LacY)[1] of *Escherichia coli* is an integral membrane protein (for a review, see ref *1*). This protein is a symporter, responsible for coupling the transport of galactosides with hydrogen ion. A stoichiometry of 1:1 (galactoside:H^+) is observed. The protein functionally and structurally acts as a monomer (*2*). Recently, an X-ray crystal structure of lacY was reported (*3*), showing a bundle of 12 transmembrane helices connected by loops that vary in length. The N-terminal set of six transmembrane segments is related by pseudosymmetry to the C-terminal set of six transmembrane segments.

Recent experiments on smaller integral membrane proteins, also consisting of transmembrane helical bundles, have revealed that transmembrane helices (*4*−*15*) and turns (*16*−*23*) behave as subdomains of the protein. Likewise, peptide fragments encoding the transmembrane helices of bacteriorhodopsin (*24*) and bovine rhodopsin (*25*) exhibited a preference for helical structure independent of the remainder of the protein as determined by nuclear magnetic resonance (NMR) in dimethyl sulfoxide (DMSO) and were consistent with the corresponding region of the crystal structure of the same protein. This experimentation led to the conclusion that useful information about secondary structure can be obtained for membrane proteins from studies of peptide fragments. Molecular dynamics simulations on transmembrane segments (TMs) have shown regions of local stability of secondary structure. For example, studies on TMs from glycophorin (*26*), bacteriorhodopsin (*27*), M2 protein from influenza A (*28*), and nicotinic acetylcholine receptor (*29*) demonstrated that TMs can exhibit sufficient local stability to fold correctly as isolated helices.

Here we report data from an integral membrane protein with a larger and potentially more conformationally flexible transmembrane helical bundle, LacY, with 12 transmembrane segments. TM1−TM11 were synthesized, and their secondary structure in solution was determined by multidimensional nuclear magnetic resonance (NMR). Molecular dynamics was carried out on all 12 TMs of LacY, comparing their conformational dynamics in DMSO to dynamics in dimyristoylphosphatidylcholine (DMPC) bilayers. In contrast to the studies mentioned above, not all the TMs exhibited stability of helical conformation throughout the segment. The sites of local instability of helical structure from molecular dynamics and from NMR studies are correlated. Mapping these regions of stable secondary structure on the crystal structure of LacY shows a marked asymmetry within the transmembrane bundle. The C-terminal group of six TMs, containing the proton conduction pathway, has intrinsically stable secondary structure, stabilized by short-range interactions. The N-terminal group of six TMs is formed from helices that are intrinsically less conformationally stable and contain residues important to substrate binding (*3*). This asymmetry in local intrinsic stability of secondary structure likely is exploited in the mechanism of transport by LacY.

† This work was supported by grants from the National Institutes of Health to P.L.Y. (GM65250) and from the BBSRC, EPSRC (via the Bionanotechnology IRC), and Wellcome Trust to M.S.P.S.

* To whom correspondence should be addressed. P.L.Y.: e-mail, yeagle@uconn.edu; phone, (860) 486-5154; fax, (860) 486-4331. M.S.: e-mail, mark.sansom@bioch.ox.ac.uk.

‡ University of Connecticut.

§ These authors contributed equally to this work.

|| University of Oxford.

[1] Abbreviations: DMPC, dimyristoylphosphatidylcholine; DMSO, dimethyl sulfoxide; LacY, lactose permease; NMR, nuclear magnetic resonance; MD, molecular dynamics; rmsd, root-mean-square deviation; TM, transmembrane segment.

10.1021/bi060355g CCC: $33.50
Published on Web 06/08/2006

Table 1[a]

sequence	structure	name
KN**TNFWMFGLFFFFYFFIMGAYFPFFPIWLHDIN**	TM1	lph1
IS**KSDTGIIFAAISLFSLLFQPLFGLLSDKL**	TM2	lph2
KR**YLLWIITGMLVMFAPFFIFIFGPLLQ**	TM3	lph3
VGSIVGGIYLGFCFNAGAPAVEAFIEKVSRRS	TM4	lph4
FGRARMFGCVGWALCASIVIMFTINNQ	TM5	lph5
NNQFVFWLGSGCALILAVLLFFAKTD	TM6	lph6
LELFRQ**PKLWFLSLYVIGVSCTYDVFDQQFANFF**	TM7	lph7
GEQGTRVFGYVTTMGELLNASIMFFAPLIINR	TM8	lph8
RIG**GKNALLLAGTIMSVRIIGSS**	TM9	lph9
ALEVVILKTLHMFEVPFLLVGCFKYITSQ	TM10	lph10
EVR**FSATIYLVCFCFFKQLAMIFMSVLAGNMYES**	TM11	lph11
FQGAYLVLGLVALGFTLISVFT	TM12	lph12

[a] Bold type shows sequence used in the MD simulations. Underlined type shows sequence used in NMR studies.

MATERIALS AND METHODS

Peptide Synthesis. Peptides with the sequences in Table 1 were utilized in these studies. Sequences in bold were used for the molecular dynamics studies. Underlined sequences were synthesized by solid-phase synthesis at Genemed (San Francisco, CA) and used for the NMR studies.

These peptide sequences were designed on the basis of previous biochemical experiments which have provided information regarding the boundaries of the transmembrane helices (*30*). The synthesized peptides were analyzed by mass spectrometry and typically showed the correct mass for the sequence and a purity of >90%, which is adequate for the NMR measurements. Synthesis for TM12 was not successful. The mass spectrum of helix 6 exhibited a very low purity, and NMR spectra of sufficient quality could not be collected.

Molecular Dynamics. All 12 transmembrane helices were extracted from the crystal structure of LacY (PDB entry 1PV6), and their secondary structure was checked using DSSP (*31*). The resulting helices were capped at their N- and C-termini with NH_2 and CO_2H, respectively. For the simulations in DMSO, each helix was solvated with DMSO in a box with dimensions of 9 nm × 9 nm × 9 nm. The system was then energy-minimized for 100 steps using the steepest descents algorithm. Cl^- ions were added where necessary to ensure overall electroneutrality. Prior to the final production run, in all cases energy minimization and 2 ns of peptide restrained molecular dynamics were performed to remove any close contacts and to relax the system. Each simulation was run for 10 ns. All the simulations employed GROMACS version 3.1.4 (www.gromacs.org) (*32*) with a time step of 2 fs under NPT conditions for 10 ns using the GROMOS96 force field (*33*). Electrostatic interactions were calculated using particle mesh Ewald (PME) (*34*) with a 1 nm cutoff for real-space calculation. A cutoff of 1 nm was used for the van der Waals interactions. The use of a long distance cutoff has been shown to be suitable for simulations of α-helix stability (*35*). Bond lengths were constrained via the LINCS algorithm (*36*). Isotropic pressure coupling was used with a compressibility of 5.2×10^{-5} bar^{-1} and a coupling time constant (τ_p) of 1 ps. DMSO and protein were coupled separately to a temperature bath at 298 K using the Berendsen thermostat (*37*) and coordinates saved every 2 ps for analysis. Simulations in DMPC bilayers were performed using the protocol described previously (*38*) and were also 10 ns in duration.

NMR Spectroscopy. All NMR spectra were recorded on a Varian INOVA-600 or 500 MHz spectrometer at 30 °C in DMSO. DMSO was used because none of these peptides are soluble in water and DMSO solubilized all the peptides. In addition, DMSO has an intermediate dielectric ($\epsilon = 48$) similar to that of the membrane−aqueous interface where folding membrane protein secondary structure has been suggested to occur, and DMSO is not known to preferentially stabilize any particular secondary structure. Studies in detergent micelles would mask the local instability that we describe here due to substantial stabilization of the helical structure by the hydrophobic effect. Previous work with analogous peptides from bacteriorhodopsin in DMSO showed that the structures obtained by NMR analysis were the same in DMSO as the structure those sequences adopted in the crystal structure of the intact protein (*17*). Standard pulse sequences and phase cycling were employed to record two-dimensional TOCSY and NOESY spectra. NOESY data were collected with mixing times of 400 ms (*39*). Previous work with other similarly sized peptides with mixing times of 150, 250, and 400 ms showed no evidence of spin diffusion, and 400 ms showed the most interactions in the NOESY spectra. In the case of helix 1, ^{15}N HSQC-NOESY and ^{15}N HSQC spectra were collected on [^{15}N]Phe-labeled peptide. The assignment table is provided as Supporting Information. All spectra were accumulated in a phase-sensitive manner using time-proportional phase incrementation for quadrature detection in F_1. Chemical shifts were referenced to the residual protons in DMSO-d_6. Sequence-specific chemical shift assignments were obtained by using amino acid β-proton chemical shift standards to assign the spin system (amino acid) type. Inter-residue αH−NH(i+1) interactions from the NOESY spectrum were used to assign the amino acid chemical shifts to a sequence position.

Structure Refinement. The sequence-specific assignment of the ^1H NMR spectrum for each peptide was carried out using standard methods employing FELIX (MSI, Inc.). Assigned NOE cross-peaks were segmented using a statistical segmentation function and characterized as strong, medium, and weak, which correspond to upper bound distance range constraints of 2.7, 3.5, and 5.0 Å, respectively. Lower bounds between nonbonded atoms were set to the sum of their van der Waals radii (approximately 1.8 Å). Pseudoatom corrections were added to interproton distance restraints where necessary (*40*). Distance geometry calculations were carried out using DYANA (*41*) within the SYBYL 6.6 package (Tripos Software Inc., St. Louis, MO). First-generation DYANA structures, 150 in total, were calculated. Energy refinement calculations (restrained minimizations/dynamics) were carried out on the best distance geometry structures using SYBYL implementing the Kollman all-atom force field. Structures were also obtained using simulated annealing on the peptides with the distance constraints obtained from the NOESY data. Simulated annealing was carried out with the Kollman All Atom force field and Kollman charges, within Sybyl. The molecule was heated to 1000 K for 1 ps followed by cooling to 200 K over the course of 1.5 ps. Ten consecutive cycles were calculated. These calculations were performed on a Silicon Graphics R10000 computer.

RESULTS

NMR Studies. We examined all 11 peptides by NMR in DMSO. It was not possible to obtain useful two-dimensional ^1H NMR data from these unlabeled peptides in detergent

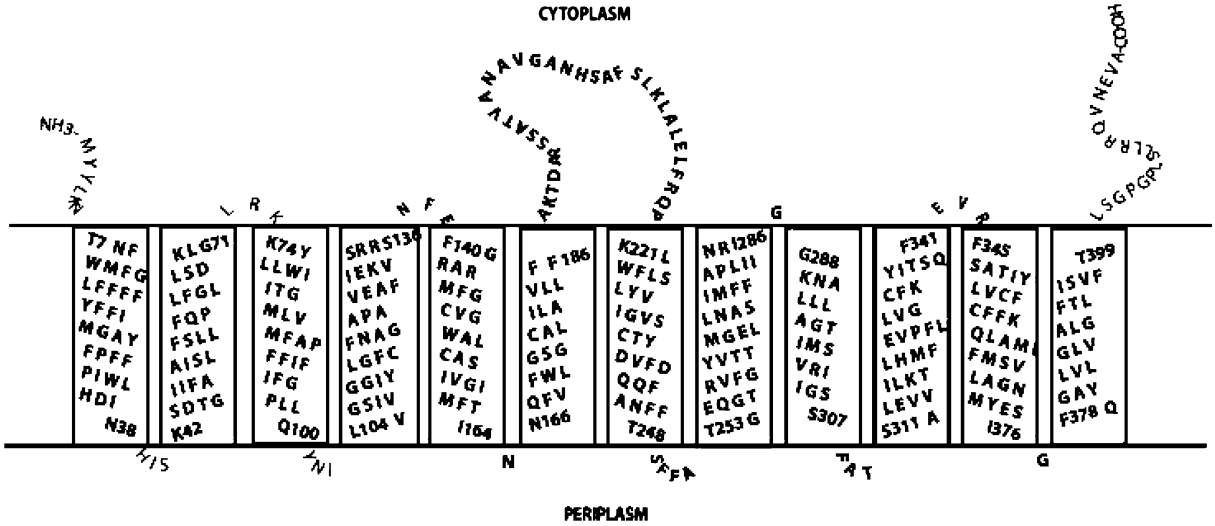

FIGURE 1: Full primary sequence of LacY organized to show the TMs (in boxes) (adapted from ref *1*).

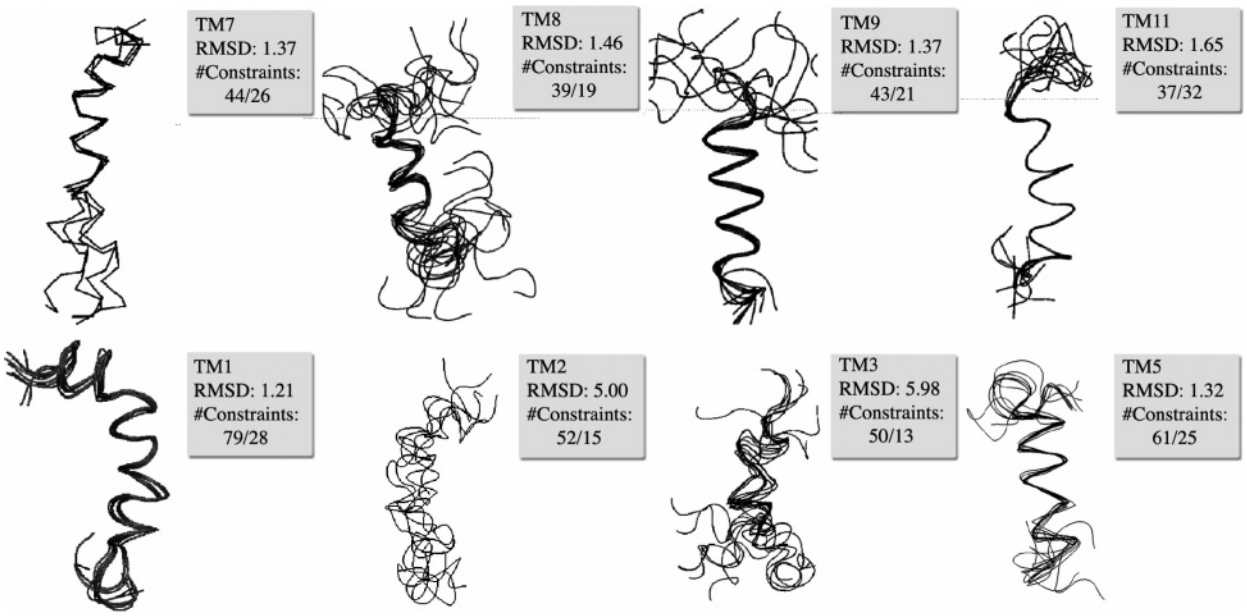

FIGURE 2: Families of DYANA structures (overlays of the best structures as determined by the target function) obtained as described in the text, for the TMs of LacY. In the boxes are the average pairwise rmsds for the family of structures and the number of constraints (intraresidue/interresidue).

micelles likely because these very hydrophobic peptides are completely buried in the micelles and experience a long rotational correlation time due to the aggregate of the detergent and the peptide. Eight of the peptides showed clear evidence of helical structure in the solution NMR studies.

Specifically, two-dimensional NMR data were used to determine the structure of the peptides in solution. An example of the NMR data from the peptide representing helix 9 is provided as Supporting Information. From the NOESY data, intraresidue, sequential, and long-range interactions were assigned to calculate the final structure. In Figure 2, the number of sequential and long-range interactions identified is listed for each peptide for which a structure was obtained. In Figure 5, the connectivity of the long-range interactions ($i-i+3$ and $i-i+4$) is displayed for each peptide. The pattern of long-range constraints is characteristic of a helical structure throughout much of the sequence of these peptides. The chemical shift index also suggests helicity in these peptides. Figure 2 shows the overlay of the family of best structures from the NMR data, and helical structures are observed through many of the sequences. The average pairwise rmsds of the backbone are listed in Figure 2. Almost all residues lie inside acceptable regions of the Ramachandran plots.

Helices 1 and 11 in solution retained features present in the crystal structure of the intact molecule. In the crystal structure, helix 1 has a bend at the Gly24/Pro28 pair. The NMR structure of the peptide corresponding to helix 1 retains this feature. Helix 11 in the crystal structure has a kink centered at Phe354. In the NMR structure of helix 11, the helix is disordered over two helical turns beginning at Phe354, after which the helix re-forms. This suggests that perhaps hydrophobic or tertiary interactions are required for the formation of helix in this region.

In contrast, helices 4 and 10 adopted random coil conformations in solution. This was evident even before structural calculation in DYANA by examination of the connectivity plots of these peptides (Figure 5). No long-range

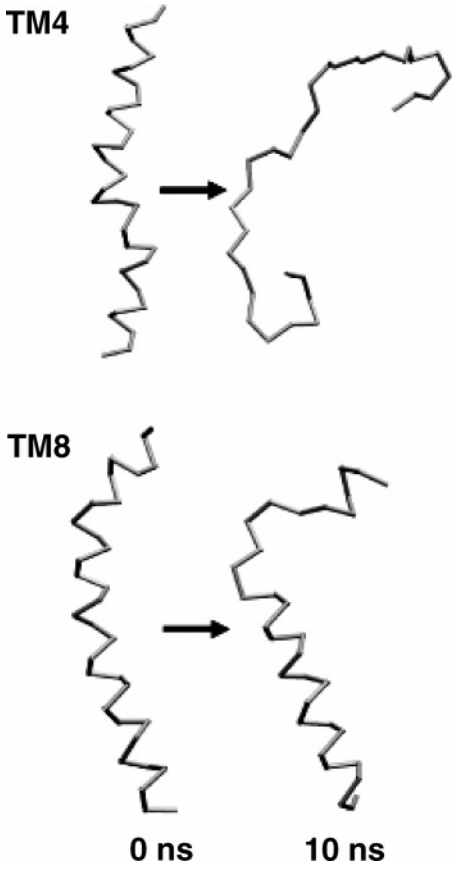

FIGURE 3: MD simulation of LacY helices. Snapshots of helices TM4 and TM8 at the start (0 ns) and end (10 ns) of each simulation are shown (as Cα traces with the C-termini being topmost). TM4 is an example of a helix that is relatively unstable in DMSO, almost completely unwinding during the simulation. In contrast, TM8 retains significant secondary structure throughout the simulation.

interactions were observed in the NOESY spectra for helix 4. Helical interactions were observed for helix 10, though too few to develop a well-ordered structure. In the region where helix 10 exhibited helical interactions in the NOESY spectra, this helix retained secondary structure in the MD simulations (see below). Helices 6 and 12 could not be chemically synthesized to the purity required for NMR study. An examination of the hydrophobicity of these helices in relation to the other helices in the molecule does not reveal any particularly unique hydrophobic character of these two helices. The hydrophobicity of helices 6 and 12 is not obviously different from those of the other helices, which suggests that the difficulty in synthesis may be due to chemical or structural features of these helices.

Molecular Dynamics Studies. Twelve transmembrane helices were extracted from the crystal structure of LacY and were separately simulated in DMSO and in DMPC bilayers for 10 ns. These helices were divided into two groups: (i) those helices (TM1, TM4−TM6, and TM12) which were relatively unstable over the duration of the DMSO simulation, resulting in substantial unfolding on a 10 ns time scale; and (ii) those helices (TM2 and TM7−TM11) that retained significant (>20%) secondary structure for the duration of the simulation. The stability plots, derived from the DSSP (*31*) analysis, are shown for both the DMSO and DMPC bilayer simulations in Figure 4. The analyses of the DMSO simulations are shown beside the NMR connectivity data in Figure 5. It is notable that four of the five most unstable helices (in DMSO) are located in the N-terminal domain of LacY. In the DMPC bilayer, on average all the helices are more stable. This suggests that the DMSO environment is needed to distinguish more fully between the α-helical propensities of the different helices. One reason may be that the bilayer environment does not permit full conformational sampling on a 10 ns time scale (*42*). However, the bilayer environment stabilizes helices in general; exposure of the polar N−H and C═O groups of the peptide bonds to a hydrophobic medium (bilayer interior) is energetically unfavorable. Hydrogen bonding in an α-helix reduces the unfavorable free energy, thus stabilizing the helix in a bilayer compared to DMSO (which has a much higher dielectric).

TM1 in the crystal has a bend at the Gly24/Pro28 pair. This produced an unstable region over the course of the simulation in DMSO, and only Tyr26 managed to retain α-helical structure. Simulation studies have shown that simple model transmembrane helices that contain a GXXXP motif may exhibit substantial flexibility (*43*). TM7 and TM11 also exhibit pronounced kinks in the crystal structure. Both TM7 and TM11 are stable over the 10 ns time scale, displaying 79 and 52% α-helicity, respectively. During the simulation, helix 7 remains kinked around Ser233 and Asp237, maintained by a side chain hydrogen bond. However, TM11 straightens out from 4 ns onward. This might imply that tertiary factors are important for this helix to kink.

TM6 and TM12 are also examples of helices that may be influenced by tertiary factors. Both these helices lie at the apical tips of the molecule, and both are unstable in the simulation. TM6 in DMSO exhibits 0% α-helicity with regions of the helix between Val169 and residue 174 becoming π-helix. Helix 12 exhibits just 5% α-helicity averaged across the 10 ns DMSO simulation. In both cases, the α-helix was converted to a mixture of π-helix and random coil during the course of the simulations.

The only helix that completely unwound (i.e., completely converted from α-helix to random coil) during the simulation was TM4. The crystal structure shows a highly kinked helix with the kink located around Pro123. Within the first 4 ns, the structure adopts a helix−turn−helix conformation, with the turn located between residues Phe118 and Val125. After 6 ns, the C-terminus unwinds to Val125, and then the helix completely unwinds in the last nanosecond of the simulation.

DISCUSSION

LacY contains a bundle of 12 transmembrane helices. Twelve peptides were designed to correspond to each of these transmembrane segments. The stability of each of these peptides was studied by NMR and molecular dynamics, and these results were compared to *B* factors from the X-ray crystal structure of the protein.

The secondary structure of 10 of these TM peptides was studied with NMR in a medium with an intermediate dielectric. Since most of these TMs are closely packed against the surfaces of other TMs in the intact protein more than against lipid hydrocarbon chains, the intermediate dielectric is more useful in assessing structural stability than is the extremely hydrophobic interior of a micelle. For TM1−TM5, TM7−TM9, and TM11, analysis of NMR data revealed a variable helix content in these fragments of LacY,

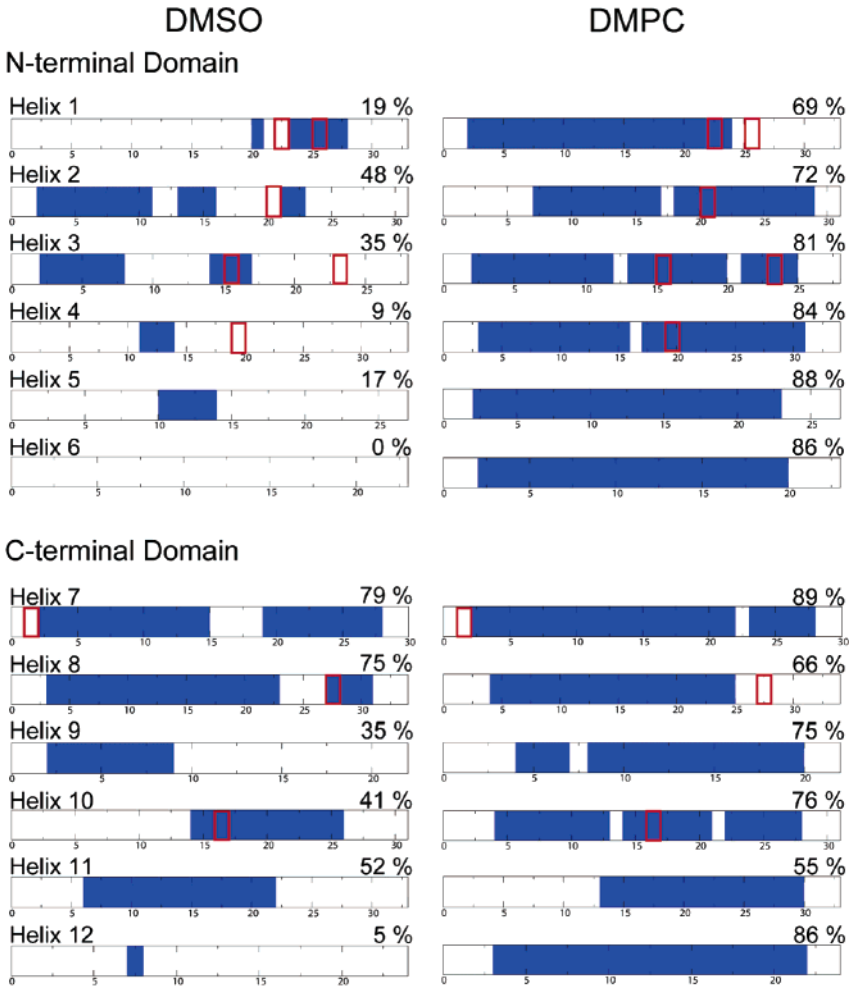

FIGURE 4: Comparison of dominant secondary structure from 10 ns MD simulations of LacY TMs in DMSO and in a DMPC bilayer. The blue bands indicate a residue that is α-helical for >80% of the simulation, as derived from secondary stucture analyses using DSSP (*31*). The red boxes denote the locations of proline residues.

from fragments containing no helix to fragments exhibiting nearly 100% helix. These data suggested that while 11 of these segments formed a helix in the crystal structure, the intrinsic stability of these fragments as a helix was non-uniform and likely depended upon the specific sequence.

Molecular dynamics simulations were employed to provide a comparative analysis. TM2, TM7, TM8, TM10, and TM11 proved to be largely stable as α-helices over the 10 ns simulation in DMSO. A correlation is observed (Figure 5) between regions found to be stable as α-helix in the MD simulations in DMSO and regions of $i-i+3$ and $i-i+4$ NOEs from the NMR data (distance constraints that are characteristic of helical conformation).

Analysis of the *B* factors from the X-ray crystal structure of lacY (*3*) also shows a correlation with the MD analysis and NMR analysis. The region containing the six N-terminal transmembrane segments shows a higher average *B* factor than the region containing the six C-terminal transmembrane segments. The *B* factor does not reflect the same properties that govern the NMR data and the MD results (this analysis is limited by the resolution of the data, 3.5 Å). Nevertheless, the *B* factor (which reflects a combination of thermal motion and static conformational disorder in the crystal) reveals an asymmetry in the structure, correlated with the relative instability noted for the N-terminal region from the NMR and MD analyses.

Therefore, the most interesting result of this study of lactose permease is that despite the pseudosymmetry in the three-dimensional structure between the N-terminal and C-terminal helical bundles, the conformational dynamics of the constituent helices of the two halves of the transmembrane domain are quite different, whether viewed through the MD results, the NMR data, or the *B* factors. In Figure 6, the regions of secondary structure stability are mapped onto the X-ray crystal structure from both the NMR and MD analyses. Much of the helical bundle in the C-terminal half of the protein exhibits local stability, as demonstrated by the formation of helical structure that is independent of the remainder of the protein. In contrast, the N-terminal half of the transmembrane helical bundle shows relatively little local structure in the absence of the membrane or the rest of the protein. These data lead us to conclude that the intrinsic stability of the secondary structure within the transmembrane domain is quite different in the two halves of the protein. We interpret the intrinsic conformational instability of an isolated TM helix in DMSO as an indicator of its potential flexibility within the intact protein structure. This flexibility may be imparted to the TM by proline, which can introduce bending and/or swiveling motions, and by the sequence -G-G-, both of which are present in TM4, one of the least stable TMs in the protein.

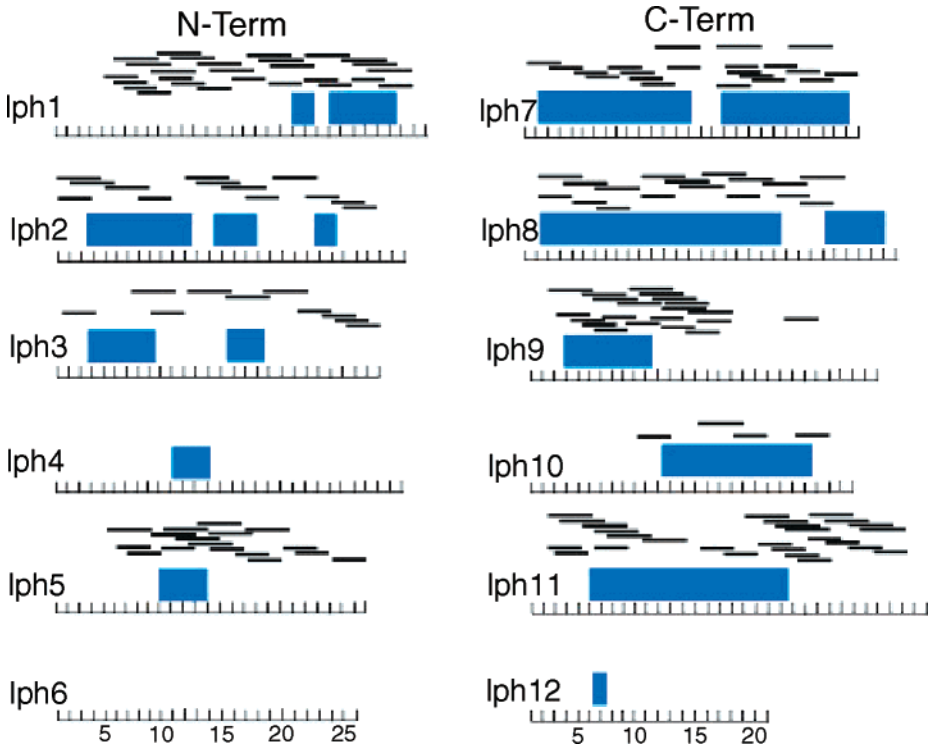

FIGURE 5: Comparison of NMR data with MD data on the TMs of LacY. The blue bands were derived from secondary structure analysis using DSSP (*31*) and designate residues that are α-helical for 80% of the 10 ns simulation. A residue that did not meet this criterion was defined as being unstructured. The NMR data of long-range constraints characteristic of helices, including $i-i+3$ and $i-i+4$ interactions, are represented by horizontal bars of connectivity between residues at each end of the bar.

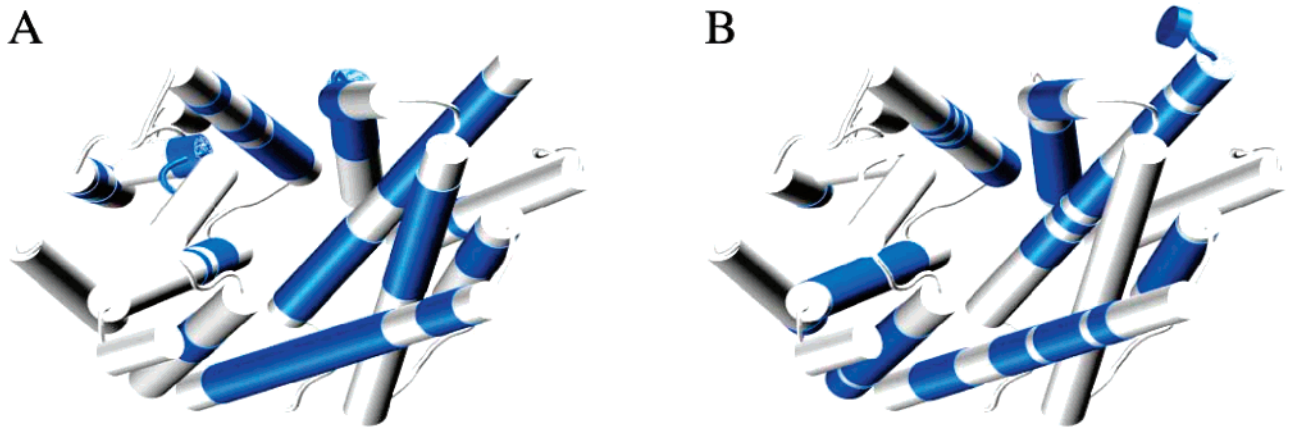

FIGURE 6: Regions of stable secondary structure (blue) mapped onto the crystal structure (1PV6). (A) Conformationally stable regions of α-helix determined from MD studies as described in the text. (B) Conformationally stable regions of α-helix identified by a density of NMR constraints as described in the text. The six N-terminal helices are on the left and the six C-terminal residues on the right.

At this point, it is wise to consider some of the technical limitations of this study. With respect to the time scales of the simulations, we recognize that only a fraction of real time is sampled in the MD simulations (tens of nanoseconds), while the NMR experiments sample conformations on the millisecond time scale (although the dipolar interactions leading to the NOEs depend on fluctuations near the nanosecond time scale). An example may be seen in the data for TM1 and TM5 in which NMR data showed α-helical regions that were not α-helical in the MD simulations (although TM1 contains some π-helices in that same region). However, the general trend for the overall domain stability is evident. Figure 5 illustrates this very well with the regions of stability observed in the MD simulations and with the NMR data. A second limitation is that these studies of isolated helices do not include any role of helix−helix interactions in the stability of the structure of TM. Currently, insufficient information is available to include such interactions in the analysis.

The rigidity of the C-terminal bundle and the flexibility of the N-terminal bundle may support the biological functions of these domains. The increased stability of the C-terminal domain reflects its role in proton translocation. A stable, rigid structural region would sample less conformational space, increasing the probability of contact between residues critical to proton transfer [Glu269, Arg302, His322, and Glu325, all in the C-terminal bundle of six helices (*3*)], and would thus be better suited to the role of proton translocation. The conformational stability of the secondary structure of proteins involved in proton translocation has been previously observed in bacteriorhodopsin. The thermostability of bacteriorhodopsin is remarkably high, with a thermal transition measured

by differential scanning calorimetry of 100 °C (*44*). Individual helices of bacteriorhodopsin are stable in organic solvent as probed by MD (*45*). As noted above, six of the seven transmembrane helices of bacteriorhodopsin are independently stable as probed by NMR, suggesting that proton-transporting proteins may benefit from well-ordered helices. The stability of the C-terminal domain of LacY is consistent with this paradigm.

In contrast to the detrimental effects of increased conformational space on proton transport, such flexibility could serve to facilitate the passage of a larger molecule such as lactose. Residues Glu126 and Arg144 are critical to substrate binding and are located in the N-terminal half of the protein, and the region containing these residues was found to be flexible in biochemical experiments (*46*). This is the same region identified in this study from structural analysis to contain relatively unstable secondary structure. The conformation of LacY shown in Figure 6 is the inward-facing mode of the protein, where the pore facing the cytoplasm is open and the periplasmic face of the protein is closed. This conformation has been termed "inward-open" (*3*). Lac permease is proposed to alternate between this conformation and the "outward-open" state, where the cytoplasmic pore is closed and the periplasmic pore is open. Lactose enters from the periplasm during the outward-open phase and binds near the salt bridge between helices 4 and 5. This binding induces the conformational change to the inward-facing conformation, after which lactose passes out of the core of lac permease and into the cytoplasm. The size of the roughly rectangular opening of the cytoplasmic pore is approximately 21 Å on its long edge (from S206 Oγ to M276 Cϵ) by 9 Å along its short edge (from F140 Cζ to F334 Cζ) in 1PV7, while the length of the TDG sugar molecule bound in the pocket is ~10.5 Å (from O3 to O3′). The cytoplasmic opening is not much larger than the sugar molecule itself. Therefore, conformational flexibility in the N-terminal domain may facilitate fluctuations in the size of the opening, which could contribute to sugar transport.

In summary, these studies offer a view beyond the static three-dimensional structure into the conformational dynamics of the protein. This combination of MD and NMR studies provides unique and valuable insight into the intrinsic conformational stability of subdomains of LacY. These studies reveal a distinct difference between the N-terminal half and the C-terminal half of the transmembrane helical bundle, in contrast to the static structural analysis that reveals only the pseudosymmetry of these two halves. This asymmetry in conformational stability likely contributes to the transport function of LacY.

ACKNOWLEDGMENT

We thank Prof. R. Kaback for initial discussions and for providing two of the peptides, John Holyoake for discussions concerning the LacY simulations, and Mark Maciejewski for assistance in the NMR experiments.

SUPPORTING INFORMATION AVAILABLE

Chemical shift assignments for helix 1 and NMR data from the peptide representing helix 9. This material is available free of charge via the Internet at http://pubs.acs.org.

REFERENCES

1. Kaback, H. R., Sahin-Toth, M., and Weinglass, A. B. (2001) The kamikaze approach to membrane transport, *Nat. Rev. Mol. Cell Biol. 2*, 610−20.
2. Sahin-Toth, M., Lawrence, M. C., and Kaback, H. R. (1994) Properties of permease dimer, a fusion protein containing two lactose permease molecules from *Escherichia coli*, *Proc. Natl. Acad. Sci. U.S.A. 91*, 5421−5.
3. Abramson, J., Smirnova, I., Kasho, V., Verner, G., Kaback, H. R., and Iwata, S. (2003) Structure and mechanism of the lactose permease of *Escherichia coli*, *Science 301*, 610−5.
4. Popot, J.-L., and Engelman, D. M. (2000) Helical Membrane Protein Folding, Stability, and Evolution, *Annu. Rev. Biochem. 69*, 881−922.
5. Lemmon, M. A., Flanagan, J. M., Hunt, J. F., Adair, B. D., Bormann, B.-J., Dempsey, C. E., and Engelman, D. M. (1992) Glycophorin A dimerization is driven by specific interactions between transmembrane α-helices, *J. Biol. Chem. 267*, 7683−9.
6. Hunt, J. F., Earnest, T. N., Bousche, O., Kalghatgi, K., Reilly, K., Horvath, C., Rothschild, K. J., and Engelman, D. M. (1997) A biophysical study of integral membrane protein folding, *Biochemistry 36*, 15156−76.
7. Berlose, J., Convert, O., Brunissen, A., Chassaing, G., and Lavielle, S. (1994) Three-dimensional structure of the highly conserved seventh transmembrane domain of G-protein-coupled receptors, *FEBS Lett. 225*, 827−43.
8. Lomize, A. L., Pervushin, K. V., and Arseniev, A. S. (1992) Spatial structure of (34−65)bacterioopsin polypeptide in SDS micelles determined from nuclear magnetic resonance data, *J. Biomol. NMR 2*, 361−72.
9. Barsukov, I. L., Nolde, D. E., Lomize, A. L., and Arseniev, A. S. (1992) Three-dimensional structure of proteolytic fragment 163−231 of bacterioopsin determined from nuclear magnetic resonance data in solution, *Eur. J. Biochem. 206*, 665−72.
10. Pervushin, K. V., Orekhov, V. Y., Popov, A. I., Musina, L. Y., and Arseniev, A. S. (1994) Three-dimensional structure of (1−71)bacterioopsin solubilized in methanol/chloroform and SDS micelles determined by ^{15}N-^{1}H heteronuclear NMR spectroscopy, *Eur. J. Biochem. 219*, 571−83.
11. Chopra, A., Yeagle, P. L., Alderfer, J. A., and Albert, A. (2000) Solution structure of the sixth transmembrane helix of the G-protein coupled receptor, rhodopsin, *Biochim. Biophys. Acta 1463*, 1−5.
12. Yeagle, P. L., Danis, C., Choi, G., Alderfer, J. L., and Albert, A. D. (2000) Three-Dimensional Structure of the Seventh Transmembrane Helical Domain of the G-protein Receptor, Rhodopsin, *Mol. Vision 6*, a17.
13. Arshava, B., Liu, S. F., Jiang, H., Breslav, M., Becker, J. M., and Naider, F. (1998) Structure of segments of a G protein-coupled receptor: CD and NMR analysis of the *Saccharomyces cerevisiae* tridecapeptide pheromone receptor, *Biopolymers 46*, 343−57.
14. Gargaro, A. R., Bloomberg, G. B., Dempsey, C. E., Murray, M., and Tanner, M. J. (1994) The solution structures of the first and second transmembrane-spanning segments of band 3, *Eur. J. Biochem. 221*, 445−54.
15. Piserchio, A., Bisello, A., Rosenblatt, M., Chorev, M., and Mierke, D. F. (2000) Characterization of parathyroid hormone/receptor interactions: Structure of the first extracellular loop, *Biochemistry 39*, 8153−60.
16. Franzoni, L., Nicastro, G., Pertinhez, T. A., Oliveira, E., Nakaie, C. R., Paiva, A. C., Schreier, S., and Spisni, A. (1999) Structure of two fragments of the third cytoplasmic loop of the rat angiotensin II AT1A receptor. Implications with respect to receptor activation and G-protein selection and coupling, *J. Biol. Chem. 274*, 227−35.
17. Katragadda, M., Alderfer, J. L., and Yeagle, P. L. (2000) Solution structure of the loops of bacteriorhodopsin closely resemble the crystal structure, *Biochim. Biophys. Acta 1466*, 1−6.
18. Mierke, D. F., Royo, M., Pelligrini, M., Sun, H., and Chorev, M. (1996) Third cytoplasmic loop of the PTH/PTHrP receptor, *J. Am. Chem. Soc. 118*, 8998−9004.
19. Yeagle, P. L., Alderfer, J. L., and Albert, A. D. (1997) The first and second cytoplasmic loops of the G-protein receptor, rhodopsin, independently form β-turns, *Biochemistry 36*, 3864−9.
20. Yeagle, P. L., Salloum, A., Chopra, A., Bhawsar, N., Ali, L., Kuzmanovski, G., Alderfer, J. L., and Albert, A. D. (2000) Structures of the Intradiskal Loops and Amino Terminus of the G-protein Receptor, Rhodopsin, *J. Pept. Res. 55*, 455−65.

21. Jung, H., Windhaber, R., Palm, D., and Schnackerz, K. D. (1995) NMR and circular dichroism studies of synthetic peptides derived from the third intracellular loop of the β-adrenoceptor, *FEBS Lett. 358*, 133−6.
22. Abdulaev, N. G., Ngo, T., Chen, R., Lu, Z., and Ridge, K. D. (2000) Functionally discrete mimics of light-activated rhodopsin identified through expression of soluble cytoplasmic domains, *J. Biol. Chem. 275*, 39354−63.
23. Gelber, E. I., Kroeze, W. K., Willins, D. L., Gray, J. A., Sinar, C. A., Hyde, E. G., Gurevich, V., Benovic, J., and Roth, B. L. (1999) Structure and function of the third intracellular loop of the 5-hyroxytryptamine (2A) receptor: The third intracellular loop is α-helical and binds purified arrestins, *J. Neurochem. 72*, 2206−14.
24. Katragadda, M., Alderfer, J. L., and Yeagle, P. L. (2001) Assembly of a polytopic membrane protein structure from the solution structures of overlapping peptide fragments of bacteriorhodopsin, *Biophys. J. 81*, 1029−36.
25. Katragadda, M., Chopra, A., Bennett, M., Alderfer, J. L., Yeagle, P. L., and Albert, A. D. (2001) Structures of the transmembrane helices of the G-protein coupled receptor, rhodopsin, *J. Pept. Res. 58*, 79−89.
26. Petrache, H. I., Grossfield, A., MacKenzie, K. R., Engelman, D. M., and Woolf, T. B. (2000) Modulation of glycophorin A transmembrane helix interactions by lipid bilayers: Molecular dynamics calculations, *J. Mol. Biol. 302*, 727−46.
27. Iyer, L. K., and Vishveshwara, S. (1996) The stability of transmembrane helices: A molecular dynamics study on the isolated helices of bacteriorhodopsin, *Biopolymers 38*, 401−21.
28. Forrest, L. R., Tieleman, D. P., and Sansom, M. S. (1999) Defining the transmembrane helix of M2 protein from influenza A by molecular dynamics simulations in a lipid bilayer, *Biophys. J. 76*, 1886−96.
29. Sankararamakrishnan, R., and Sansom, M. S. (1995) Structural features of isolated M2 helices of nicotinic receptors. Simulated annealing via molecular dynamics studies, *Biophys. Chem. 55*, 215−30.
30. Wolin, C. D., and Kaback, H. R. (2001) Functional estimation of loop-helix boundaries in the lactose permease of *Escherichia coli* by single amino acid deletion analysis, *Biochemistry 40*, 1996−2003.
31. Kabsch, W., and Sander, C. (1983) Dictionary of protein secondary structure: Pattern recognition of hydrogen-bonded and geometrical features, *Biopolymers 22*, 2577−637.
32. Lindahl, E., Hess, B., and van der Spoel, D. (2001) GROMACS 3.0: A package for molecular simulation and trajectory analysis, *J. Mol. Modell. 7*, 306−17.
33. Hermans, J., Berendsen, H. J. C., van Gunsteren, W. F., and Postma, J. P. M. (1984) A consistent empirical potential for water−protein interactions, *Biopolymers 23*, 1513−8.
34. Darden, T., York, D., and Pedersen, L. (1993) Particle mesh Ewald: An N.log(N) method for Ewald sums in large systems, *J. Chem. Phys. 98*, 10089−92.
35. Weber, W., Hunenberger, P. H., and McCammon, J. A. (2000) Molecular dynamics simulations of a polyalanine octapeptide under Ewald boundary conditions: Influence of artificial periodicity on peptide conformation, *J. Phys. Chem. B 104*, 3668−75.
36. Hess, B., Bekker, H., Berendsen, H. J. C., and Fraaije, J. B. E. M. (1997) LINCS: A linear constraint solver for molecular simulations, *J. Comput. Chem. 18*, 1463−72.
37. Berendsen, H. J. C., Postman, W. F., van Gunsteren, W. F., DiNola, A., and Haak, J. R. (1984) Molecular dynamics with coupling to an external bath, *J. Chem. Phys. 81*, 3684−90.
38. Ulmschneider, M. B., Tieleman, D. P., and Sansom, M. S. P. (2004) Interactions of a transmembrane helix and a membrane: Comparative simulations of bacteriorhodopsin helix A, *J. Phys. Chem. B 108*, 10149−59.
39. Kumar, A., Ernst, R. R., and Wüthrich, K. (1980) A two-dimensional nuclear Overhauser enhancement (2D NOE) experiment for the elucidation of complete proton−proton cross-relaxation networks in biological macromolecules, *Biochem. Biophys. Res. Commun. 95*, 1−6.
40. Wüthrich, K., Billeter, M., and Braun, W. J. (1983) Pseudo-structures for the 20 common amino acids for use in studies of protein conformations by measurements of intramolecular proton proton distance constraints with nuclear magnetic resonance, *J. Mol. Biol. 169*, 949−61.
41. Guntert, P., Braunk, W., and Wüthrich, K. (1991) Efficient computation of three-dimensional protein structures in solution from NMR data using the program DIANA and the supporting programs CALIBA, HABAS, and GLOMSA, *Mol. Biol. 217*, 517−30.
42. Faraldo-Gómez, J. D., Forrest, L. R., Baaden, M., Bond, P. J., Domene, C., Patargias, G., Cuthbertson, J., and Sansom, M. S. P. (2004) Conformational sampling and dynamics of membrane proteins from 10-nanosecond computer simulations, *Proteins: Struct., Funct., Bioinf. 57*, 783−91.
43. Bright, J. N., and Sansom, M. S. (2003) The flexing/twirling helix: Exploring the flexibility about molecular hinges formed by proline and glycine motifs in transmembrane helices, *J. Phys. Chem. B 107*, 627−36.
44. Jackson, M. B., and Sturtevant, J. M. (1978) Phase transitions of the purple membranes of *Halobacterium halobium*, *Biochemistry 17*, 911−5.
45. Efremov, R. G., Nolde, D. E., Vergoten, G., and Arseniev, A. S. (1999) A solvent model for simulations of peptides in bilayers. II. Membrane-spanning α-helices, *Biophys. J. 76*, 2460−71.
46. Weinglass, A. B., and Kaback, H. R. (1999) Conformational flexibility at the substrate binding site in the lactose permease of *Escherichia coli*, *Proc. Natl. Acad. Sci. U.S.A. 96*, 11178−82.

BI060355G